Organization of stratification, turbulence, and veering in bottom Ekman layers

A. Perlin,[1] J. N. Moum,[1] J. M. Klymak,[1,2] M. D. Levine,[1] T. Boyd,[1] and P. M. Kosro[1]

Received 3 August 2004; revised 17 November 2006; accepted 7 December 2006; published 24 May 2007.

[1] Detailed observations of the Ekman spiral in the stratified bottom boundary layer during a 3-month period in an upwelling season over the Oregon shelf suggest a systematic organization. Counter-clockwise veering in the bottom boundary layer is constrained to the weakly stratified layer below the pycnocline, and its height is nearly identical to the turbulent boundary layer height. Veering reaches 13+/−4 degrees near the bottom and exhibits a very weak dependence on the speed and direction of the interior flow and the thickness of the veering layer. A simple Ekman balance model with turbulent viscosity consistent with the law-of-the-wall parameterization modified to account for stratification at the top of the mixed layer is used to demonstrate the importance of stratification on the Ekman veering. The model agrees reasonably well with observations in the lower 60–70% of the bottom mixed layer, above which it diverges from the data due to the unaccounted physics in the interior. Neglect of stratification in an otherwise identical model results in far worse agreement with the data yielding veering in the bottom Ekman layer which is much smaller than measured, but distributed over a much thicker layer.

Citation: Perlin, A., J. N. Moum, J. M. Klymak, M. D. Levine, T. Boyd, and P. M. Kosro (2007), Organization of stratification, turbulence, and veering in bottom Ekman layers, *J. Geophys. Res.*, *112*, C05S90, doi:10.1029/2004JC002641.

1. Introduction

[2] Friction in the bottom boundary layer (BBL) of the ocean causes ageostrophic transport perpendicular to the interior flow. This was first explored by Ekman, who arrived at a solution for the velocity profile by considering a momentum balance of three terms: the Coriolis force, the horizontal pressure gradient, and a vertical shear stress. This bottom Ekman transport is of particular interest on continental shelves, such as off Oregon, because it helps drive the upwelling of deep, nutrient-rich near-bottom water during southwards geostrophic flow (see *Kundu* [1976], *Huyer and Smith* [1978], and *Perlin et al.* [2005a] for a recent example on the Oregon Coast).

[3] Few observational tests of Ekman theory have been made in the bottom boundary layer because the velocities are small and measurements near the bottom are difficult to make. The constant viscosity BBL theory predicts that, as the bottom is reached, the direction of the current will have veered 45° counter-clockwise (N. Hemisphere) from the direction of the interior geostrophic velocity. Observations of oceanic bottom Ekman layers, however, indicate that the counter clockwise veering over the BBL is much less than 45°, typically reaching a maximum of only 20° (Table 1).

[4] The length scale of the neutrally stratified bottom Ekman layer is often given by $D_E = \gamma u_*/f$ with the proportionality constant γ of order 1, where f is the Coriolis parameter, u_* is the friction (characteristic) velocity in the bottom boundary layer defined as $u_* = \sqrt{\tau_b/\rho}$, τ_b is the bottom stress, and ρ is density. The length scale D_E can be derived from the momentum balance [*Cushman-Roisin*, 1994] by assuming that the Ekman number (ratio of horizontal stress to Coriolis force) is of order one: $\frac{K_v}{fD_E^2} \sim 1$, where K_v is the eddy viscosity, and by assuming that $K_v \sim u_* D_E$, which comes from turbulence theory where D_E is also the scale of the largest turbulent eddies. Previous work has used this scale to characterize the veering thickness, and have often found values of γ near 0.4 (Table 1).

[5] In classic Ekman theory, the distributions of velocity and veering are calculated assuming a constant eddy viscosity near the boundary. However, turbulence theory and observations in unstratified boundary layers indicate that the eddy viscosity near a boundary is given by the law-of-the-wall in which the eddy viscosity is proportional to the distance from the boundary. *Cushman-Roisin and Malačič* [1997] (hereafter CRM) solve the bottom Ekman layer with the law-of-the-wall eddy viscosity and predict much smaller veering angles than the constant eddy viscosity solution. This parameterization has also been used by *Ellison* [1956] for the atmospheric boundary layer, by *Madsen* [1977] in a study of the surface Ekman layer, and by many others in studies of tidal currents in shallow well-mixed waters.

[6] A further complication to the classic Ekman theory is the presence of stratification, which suppresses velocity fluctuations and thus turbulence in the boundary layer,

[1]College of Oceanic and Atmospheric Sciences, Oregon State University, Corvallis, Oregon, USA.
[2]Now at School of Earth and Ocean Sciences, Department of Physics, University of Victoria, Victoria, British Columbia, Canada.

0148-0227/07/2004JC002641$09.00

Table 1. Observations of Bottom Ekman Layer

Reference	Location and Duration of the Experiment	Veering	Height of the Ekman Layer	Notes
Weatherly [1972]	Straits of Florida; 155 hours	10°	—	Array of current meters. Veering is registered only between current meters at 1 and 3 m above the bottom.
Mercado and Van Leer [1976]	Florida shelf;	13°-18°	$(0.3–0.4)\frac{u_*}{f}$, where u_* is the friction velocity and f is the Coriolis parameter	Temperature, conductivity and velocity data with 5 m vertical resolution to within 5 m from the bottom. Estimation of friction velocity is based on assumption of simple Ekman layer momentum balance.
Kundu [1976]	Oregon coast; 1 and 2 months	~6°	—	Measurements with current meters 5 and 20 m above the bottom.
Dickey and Van Leer [1984]	Peruvian shelf; 2 days	23°	Up to 35 m	Temperature, conductivity and velocity data with 3 m vertical resolution to within 3 m from the bottom.
Saylor and Miller [1988]	Lake Michigan; 4 months	11°	—	Array of current meters 1–9 m and 50 m above the bottom. Veering is registered between 1 and 9 m above the bottom.
Saylor [1994]	Lake Michigan	20° for strong currents	20 to 100 m.	The same as above plus ADCP (Acoustic Doppler Current Profiler) data. Ekman layer thickness is estimated as $0.4u_*/f$, when u_* is computed from log profile using current meters data.
Lass and Mohrholz [2003]	Arkona Basin (Baltic Sea); two winter seasons	—	5–15 m	Ekman layer is contained below the strong halocline.

and, in turn, influences velocity veering. *Pollard et al.* [1973] have argued that in the presence of stratification, the height of the Ekman layer is governed not by u_*/f, but by $u_*/\sqrt{Nf}$ when $N \geq f$, where N is the stratification of the layer adjacent to the mixed layer, representing the ambient stratification. Observational evidence of the modification of the Ekman layer in the presence of stratification can be found elsewhere. For example, *Price and Sundermeyer* [1999] showed that the Ekman spiral in the surface boundary layer was thinned by stratification and that the wind-driven transport was trapped mainly within the upper part of the Ekman layer. *Weller and Plueddemann* [1996] showed that the Ekman transport was concentrated above the pycnocline and was divided almost equally between the surface mixed layer and a weakly stratified layer immediately below, and that the diurnal cycle in mixed layer height affects the velocity structure inside the Ekman layer.

[7] We have recently suggested a modification to the law-of-the-wall (MLW) that is intended to account for the suppression of turbulence by stratification away from the boundary but within an unstratified boundary layer [*Perlin et al.*, 2005b]. We have concluded that the MLW predicts significantly different velocity and turbulence dissipation profiles than the law-of-the-wall theory and agrees reasonably well with the measured data in the lower 60–70% of the bottom mixed layer (versus 20–30% for the law-of-the-wall). We have arrived at this conclusion by comparing the measured and modeled velocity and turbulence dissipation rates profiles. Here we extend this analysis to consider rotation and apply the MLW in the form of eddy viscosity formulation to investigate Ekman veering.

[8] Specifically, we demonstrate that in the presence of stratification, Ekman veering coincides with a clearly defined turbulent layer. Most of the Ekman transport occurs inside the well-mixed layer, but also extends into a weakly stratified layer above. Data from a broad, relatively flat region of the BBL on the Oregon Shelf are analyzed. The data, discussed in section 3, include 3 months of high-resolution measurements of velocity to within 2.75 m of the sea floor, supplemented by 50 h of intensive turbulence and density profiling measurements to within 2 cm of the sea floor. From these data we quantify the veering angle and the veering layer height and evaluate dependence of these properties on the interior current velocity and the level of turbulence in the BBL. The veering rate (change in veering angle/veering layer height) has been shown to be nearly inversely proportional to the veering layer height, so that the maximum veering angle has only a very weak dependence on interior flow velocity and thickness of the BBL. Our observations have been compared to solutions of the Ekman balance using both the law-of-the-wall (CRM) and the modified law-of-the-wall [*Perlin et al.*, 2005b] parameterizations of eddy viscosity.

2. Definitions and Theory

[9] The BBL typically exhibits weaker stratification and higher turbulence than the interior. To characterize the state of the BBL, we define four length scales based on observational criteria (Figure 1). The bottom mixed layer (D) is defined as the distance from the bottom over which the potential density decreases by 6×10^{-4} kg m^{-3} from its

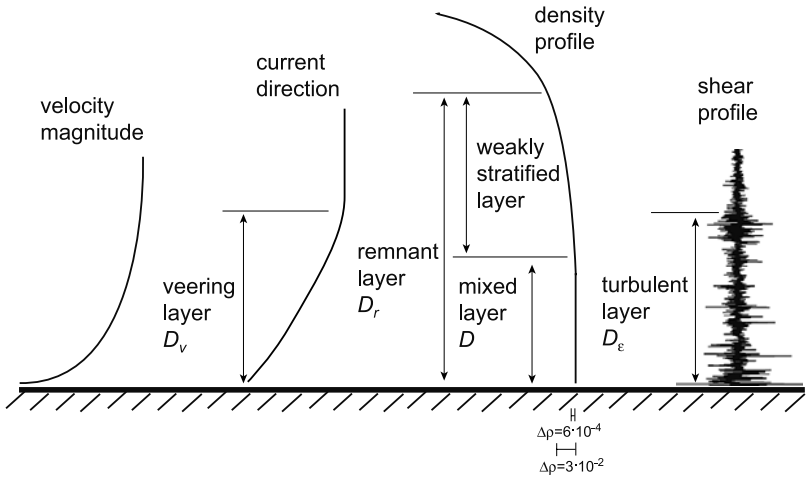

Figure 1. Schematic diagram of different BBL definitions discussed in the text.

value at the bottom. To avoid the effects of local overturns in the estimation of D, we also require the density difference to remain below this threshold value for at least 1 m. Above the mixed layer there often lies a weakly stratified layer. The combined mixed and weakly stratified layers is termed the remnant layer (D_r), and its thickness is defined as the distance from the bottom over which the potential density decreased by 3×10^{-2} kg m^{-3}. At least during upwelling conditions, the top of the remnant layer marks the lower boundary of the pycnocline. The turbulent bottom layer (D_ε) is defined as the height above the bottom at which the turbulence dissipation rate decreases to 6×10^{-9} m^2 s^{-3}. For further details and discussion of mixed, remnant and turbulent layer definitions, see *Perlin et al.* [2005a]. We define the veering layer (D_v) as the layer that contains a systematic counter-clockwise rotation of the current vector with depth (see section 4).

[10] Neglecting time dependence, nonlinear accelerations and baroclinic pressure gradients, the horizontal momentum balances in the bottom Ekman layer are given by:

$$-f(v_e - \bar{v}) = \frac{\partial}{\partial z}\left(K_v \frac{\partial u_e}{\partial z}\right) \tag{1}$$

$$fu_e = \frac{\partial}{\partial z}\left(K_v \frac{\partial v_e}{\partial z}\right), \tag{2}$$

where the interior geostrophic flow $\bar{v}$ is in the direction of the y-coordinate, (u_e, v_e) are velocity components inside the Ekman layer, the stress is parameterized by an eddy viscosity K_v, and z is the height above the bottom. The boundary conditions are

$$u_e \to 0, \quad v_e \to \bar{v}, \quad \text{as} \quad z \to \infty \tag{3}$$

$$u_e = 0, \quad v_e = 0, \quad \text{at} \quad z = z_0, \tag{4}$$

where z_0 is a constant of integration (frequently termed a roughness length) and is determined when the system of equations (1)–(4) is solved given a specified $K_v(z)$, $\bar{v}$, and bottom stress.

[11] We consider two possibilities for the specification of $K_v(z)$. First we consider K_v given by the law-of-the-wall,

$$K_v = u_* \ell, \quad \ell = \kappa z, \tag{5}$$

where κ is von Kármán's constant (=0.4), and ℓ is a turbulence length scale which increases without bound as z goes to infinity. The analytical solution of (1)–(5) is given by CRM. Second, we use the modified law-of-the-wall, where a stratified boundary layer has an outer length scale h_d that limits the growth of ℓ. The MLW eddy viscosity is given by:

$$K_v = u_* \ell, \quad \ell = \kappa z(1 - z/h_d), \tag{6}$$

for $z \le h_d$ and $K_v = 0$ for $z > h_d$. The value of h_d is chosen to be the largest value such that $\ell(z) \le \ell_o(z)$ at all depths, where the effect of stratification limiting the scale of turbulence is represented by $\ell_o = \sqrt{\varepsilon/N^3}$, the Ozmidov scale, ε is the turbulence dissipation rate and N is the buoyancy frequency at the top of the mixed layer [*Perlin et al.*, 2005b]. Since $\ell_o \to \infty$ within the mixed layer D, the value of h_d is determined by the vertical profile of ℓ_o just above D. Based on examination of many profiles on the Oregon shelf, we find $h_d \approx D^2/(D - 1)$ to be a good approximation [*Perlin et al.*, 2005b].

3. Overview of the Data

[12] The observations used in this study come from a three-month long mooring deployment and a 50-h vertical profiling time series over the Oregon shelf during the summer upwelling season of 2001, as part of the Coastal Ocean Advances in Shelf Transport (COAST) program [*Barth and Wheeler*, 2005]. The mooring was deployed in 81 m of water (45° 0.01′ N, 124° 7.00′ W) directly offshore (west) of Cascade Head [*Boyd et al.*, 2002]. Currents were observed with two acoustic Doppler profilers: an upward-looking RDI 300 kHz ADCP 4 m above the bottom with 2 m vertical resolution, and a downward-looking Nortek 2 MHz

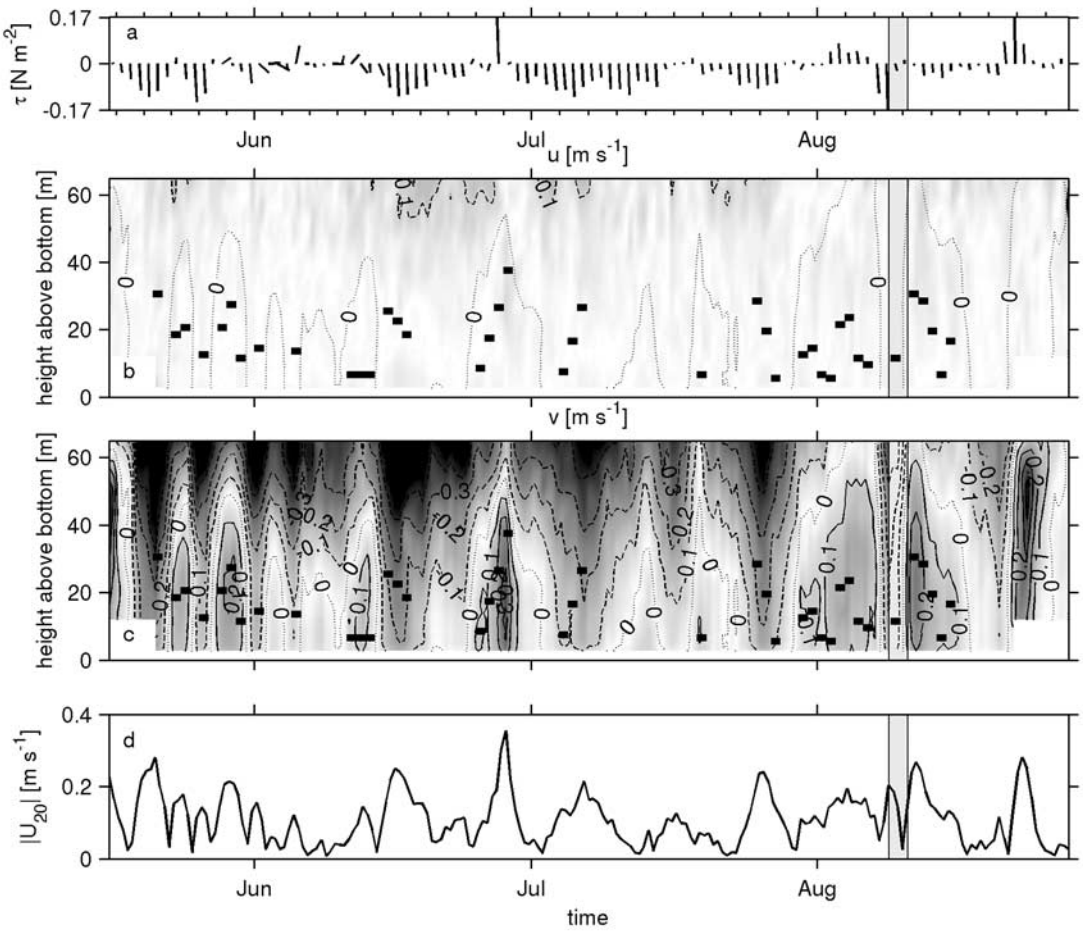

Figure 2. Time series from the mooring located at 45°0.01′ N, 124°7.00′ W, from 16 May to 28 Aug, 2001, which measured (a) wind stress, (b) eastward velocity, (c) northward velocity, and (d) velocity magnitude 20 m above the bottom. Data have been smoothed by 1 day averages. A 50-h Chameleon profiler time series was started 8 August (gray box). Veering layer height is shown on (b) and (c) with thick black line, defined only when the speed exceeds 0.05 m/s at 8 m above bottom and there are no reversals of northward velocity during averaging period.

Aquadopp profiler 9 m above the bottom with 0.5 m vertical resolution. Due to side-lobe interference and acoustic spreading, there are no reliable velocity data within 2.75 m of the bottom.

[13] The moored velocity data contain tidal and inertial oscillations. To isolate the low frequency characteristics of the BBL, daily averages of the 3-month data set were computed (Figure 2). Daily averages do not differ significantly from the 25-h low-passed filtered velocity (Chebychev, fourth order). Filtered velocity gives very similar results if used for further analysis. We opted to use daily averages for convenience. The flow has been predominantly southward (upwelling favorable), but with occasional relaxations, and even a large reversal in late June (Figure 2c). Data included in the analysis that follows come from only those daily averages during which there were no alongshore flow reversals. Since Ekman transport calculations are sensitive to erratic veering angles at low speeds, all profiles with a speed smaller than 0.05 m s^{-1} at 8 m above the bottom have been excluded from the analysis.

[14] The turbulence profiler Chameleon was used to obtain a 50-h time series near the mooring, measuring turbulence dissipation rate, temperature and conductivity. A detailed description of Chameleon and the procedures used to process the data can be found in *Moum et al.* [1995]. Chameleon has been routinely run into the bottom, permitting profiles to within 2 cm of the seabed, which is a necessary condition for estimating bottom stress [*Perlin et al.*, 2005b]. The time series starts during a period of high southward flow (Figure 3d) that has reversed 36 h into the observation. The mixed layer (D) was thicker (~20 m) during the strong flow conditions, thinning to less than 10 m as the flow slowed (Figure 3a). The turbulence was also larger during the high flow, and the thickness of the turbulent layer (D_ε) roughly followed the mixed layer thickness (Figure 3b).

[15] To relate the observations to the momentum balance (1)–(4), two quantities are needed: u_* and $\overline{v}$. u_* has been estimated directly from the profiles of turbulent dissipation $\varepsilon(z)$ using the dissipation method $u_* = \langle \varepsilon \kappa z \rangle^{1/3}$. This method for computing the friction velocity is described by *Dewey and*

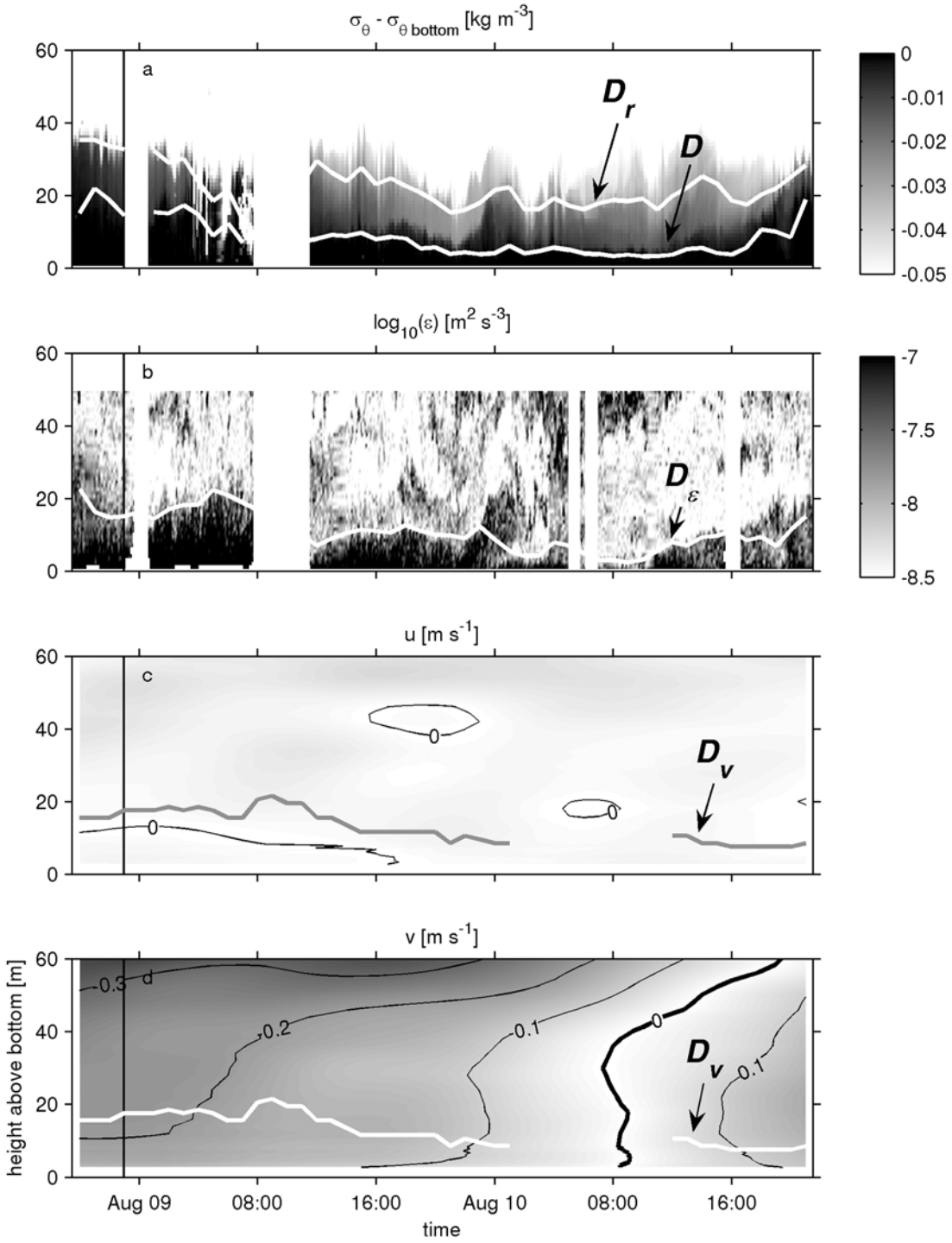

Figure 3. Data from 50-h Chameleon time series collected near the mooring showing (a) 1-h averaged density (white lines mark mixed and remnant layer heights), and (b) 1-h averaged turbulence dissipation rate (white line marks turbulent layer height). Data from the mooring show (c) low-passed (second-order Butterworth 21h) eastward velocity (gray line marks veering layer height) and (d) low-passed (second-order Butterworth 21h) northward velocity (white line marks veering layer height). Vertical line marks the time of the profile shown in Figure 6.

Crawford [1988] and discussed by *Perlin et al.* [2005b] for this same data set. Direct estimates of u_* cannot be made from the mooring data; however, two indirect estimates can be made based on the velocity time series. The first method is based on the quadratic drag approximation, $u_{*20} = \sqrt{C_D U_{20}^2}$, where U_{20} is the velocity measured 20 m above the bottom. *Perlin et al.* [2005b] have found that for this shelf as a whole C_D varies between 4.5×10^{-4} and 1.6×10^{-3},

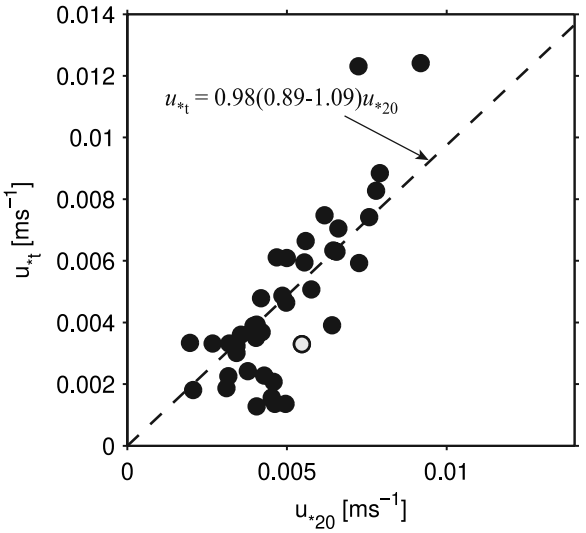

Figure 4. Friction velocity computed from Ekman transport u_{*t} vs. friction velocity computed from current velocity 20 m above the bottom u_{*20}. Linear regression is shown by dashed line, and 95% confidence limits for the linear regression are shown in brackets.

with an average of 10^{-3}. The second method assumes that $\tau_b \sim \tau_{yb}$ and estimates u_{*t} from the Ekman transport normal to the interior geostrophic flow $\bar{v}$ as $u_{*t} \sim \sqrt{\tau_{yb}/\rho} = \sqrt{\vartheta_{Ek} f}$, where $\vartheta_{Ek} = \int_{z_0}^{D_v} u_e dz$. Note that since there are no data below 2.75 m, we calculate the integral using extrapolated $u_e(z)$ based on the law-of-the-wall. The two estimates of u_* are well correlated ($r_{u_{*t}/u_{*20}} = 0.8(0.65 - 0.89)$) with $\frac{u_{*t}}{u_{*20}} = 0.98(.89 - 1.09)$ (Figure 4).

[16] The interior geostrophic velocity $\bar{v}$ is taken to be the velocity observed from the mooring at the top of the veering layer at height D_v (defined in the next section) and hence $u_e(D_v) = 0$. Note that the direction of $\bar{v}$ varies slowly as a function of time, although it is most often aligned in a nearly north-south direction.

4. Veering Layer

[17] Owing to the Earth's rotation, the current veers in a counter-clockwise direction as the bottom is approached from the geostrophic interior flow. The veering is defined to be contained within the veering layer D_v. The challenge is to distinguish between the veering which is induced by the presence of the bottom boundary and the veering that may be caused by other motions in the interior based on the velocity observations. To accomplish this, the veering layer thickness D_v has been estimated as follows. The upper limit has been chosen at the height $h_{\max} = 0.6\frac{u_*}{f}$ above the bottom. The veering rate has been calculated as the change in the angle over a 5 meter interval from h to $(h - 5$ m). If at a height h the veering rate exceeds the threshold value of $6/h$ (deg/m), we set $D_v = h$. If not, then the veering rate over 5 m is repeatedly calculated at successively deeper depths. The threshold has been defined such that the veering rate at $z = D_v$ is large enough to result in at least 6 degrees of veering when extrapolated from D_v to the sea floor. This definition was based on extensive analysis of the individual veering angle profiles. The threshold was defined to be small enough to identify veering layers with smaller than average rotation, but large enough to exclude random variation in direction of the velocity above the Ekman layer. Varying the threshold value from $1/h$ to $11/h$ (deg/m) leads to at most a 1 m root mean square (RMS) difference in the height of the veering layer (Figure 5), which is only a 20% difference for the thinnest veering layers.

[18] An example of the veering of the velocity in a single profile is shown in Figure 6a. The interior current is slightly above 0.2 m s^{-1} and flows 185 degrees clockwise from north. Counter-clockwise veering starts approximately at $D_v = 19$ m and reaches $\sim 12°$ at 2.75 m above the bottom (below which we have no velocity measurements). The turbulence is high near the bottom (Figure 6b), and the water is well-mixed (Figure 6c). The veering, in this example, starts at the depth at which the turbulence is high.

[19] It is only during the 50-h Chameleon time series that we can obtain estimates of D, D_r, and D_ε. During this period, the veering height D_v follows the turbulent layer thickness (D_ε) (Figure 7). Also, $D_r \cong 2D_v$, $D \cong 2/3D_v$. D_v compares to the Ekman length scale for neutrally stratified boundary layers u_*/f with coefficient of proportionality $\gamma \approx 0.26$, and the stratified Ekman length scale $u_*/\sqrt{Nf}$ with coefficient of proportionality $\beta \approx 1.6$ (*Pollard et al.* [1973] suggested $\beta = 2^{3/4} \approx 1.7$). In the case of the latter scaling, the stratification in the weakly stratified layer above D has been used (if stratification over D_r were applied, $\beta \approx 1.5$).

[20] Stratification can suppress turbulence on a shorter than tidal time scale, which would affect the Ekman spiral, as has been shown by *Price and Sundermeyer* [1999], and *Weller and Plueddemann* [1996]. It is extremely difficult however to decompose very noisy unfiltered data into flow related to internal tides and to Ekman dynamics in order to

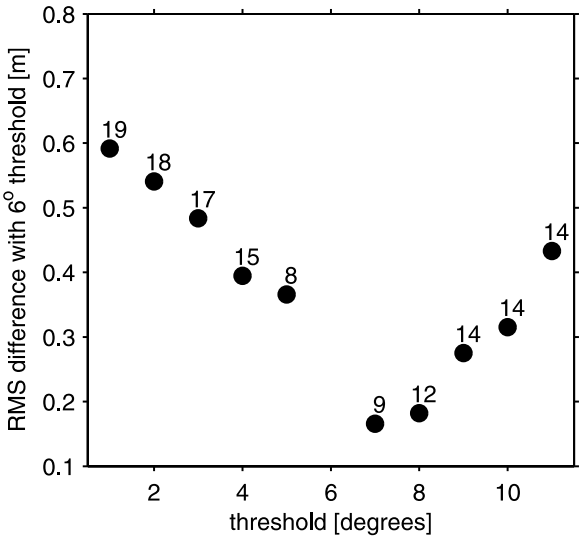

Figure 5. Mean RMS difference between the veering layer heights compared for the thresholds 1°–11°, and for the 6° threshold. Numbers above the dots indicate number of profiles where selected veering layer height is different from 6° threshold (out of 40 total).

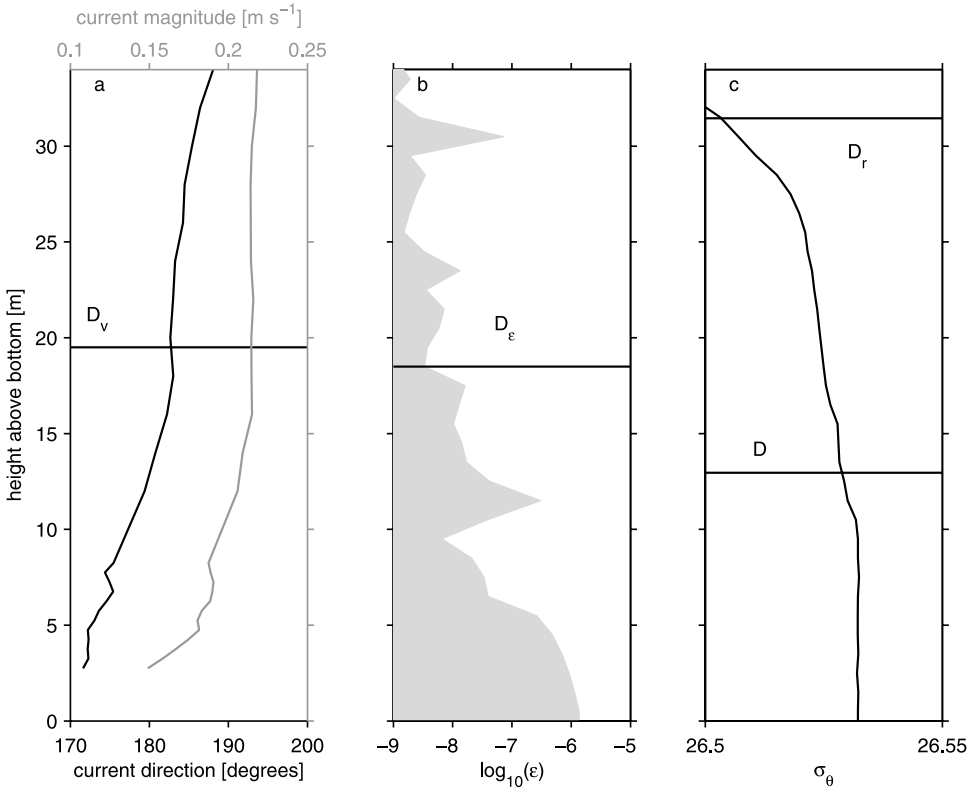

Figure 6. An example Chameleon profile on 8 August 2001, 23:00 showing (a) profiles of velocity magnitude (gray) and direction (black) (veering layer height is marked at 19.5 m), (b) turbulent dissipation rate (turbulent layer height is marked at 18.5 m), and (c) density profile (mixed layer height is marked at 13 m and remnant layer height is marked at 32 m).

select D_v. We calculated D_v from filtered velocity profiles. Hence, hourly D_v values cannot be considered to be independent. Since the number of degrees of freedom for D_v is very small, quantifying its correlation with other boundary layer scales is problematic.

[21] We extend the analysis over the 3-month mooring record to examine the consistency of both the veering angle and the cross-axis velocity (u_e) with current direction, speed and veering layer thickness. Since there were no turbulence observations from which to obtain a direct estimate of u_*, the indirect estimates of bottom stress, u_{*t} and u_{*20}, have been used (see section 2). The veering thickness D_v has been found to be highly correlated with both estimates of u_* such that $r_{D_v/u_{*20}} = 0.84(0.71 - 0.91)$ and $r_{D_v/u_{*t}} = 0.9(0.81 - 0.95)$ with linear regression $D_v \approx 0.36u_{*20}/f \simeq 0.35u_{*t}/f$ and mean ratio $D_v/(u_{*20}/f) \approx 0.34(0.31 - 0.37)$ and $D_v/(u_{*t}/f) \approx 0.39(0.35 - 0.44)$ (Figure 8). The proportionality constant of 0.35 is slightly higher than 0.26 which appears to be a good fit over the 50 h period (Figure 7) when u_*/f can be estimated directly from observed dissipation (see open circles in Figure 8 for the times corresponding to the time series).

[22] To study the observed veering angles of profiles made at a variety of flow conditions and different values of D_v it is useful to define the average veering angle by:

$$\alpha_{av}(z/D_v) = \left\langle \tan^{-1} \frac{-u_e(z)\, v_e(D_v)}{v_e(D_v)\, v_e(z)} \right\rangle \qquad (7)$$

where the operator $< \cdots >$ is the arithmetic average of the angles at height z. This quantity is sensitive to erratic veering angles at low speeds, so flows with speed less than 0.05 ms^{-1} measured 8 m above the bottom are not considered. This averaging is different from a true vector average. However, at speeds above 0.05 ms^{-1}, the methods do not differ significantly.

[23] The average veering angle profile $\alpha_{av}(z/D_v)$ is remarkably constant for the duration of the 3-month time series (Figure 9). Since the daily average flow is nearly parallel to the coast, the observations can be divided into average flows that are either generally southward or northward with corresponding upslope or downslope Ekman flow. Shutdown time for our Ekman flow computed as in *Garrett et al.* [1993] is of the order of hours to a day, implying differences between the upslope and downslope Ekman flows. We have however demonstrated [*Perlin et al.*, 2005a] that upwelling in the BBL could continue for a few days without being arrested, and that a simple 2D Ekman balance is roughly satisfied in the BBL at this location on the Oregon shelf. Our observations of Ekman veering confirm that finding: the difference in average veering angle between southward flow (upslope Ekman flow) and northward flow (downslope Ekman flow) is statistically insignificant (Figure 9a). Also, there are no appreciable differences in α_{av} between thick ($D_v > 10$ m) and thin ($D_v < 10$m) veering layers (Figure 9b). Differences in α_{av} between high flow ($U_{20} > 15$ cm/s) and low flow

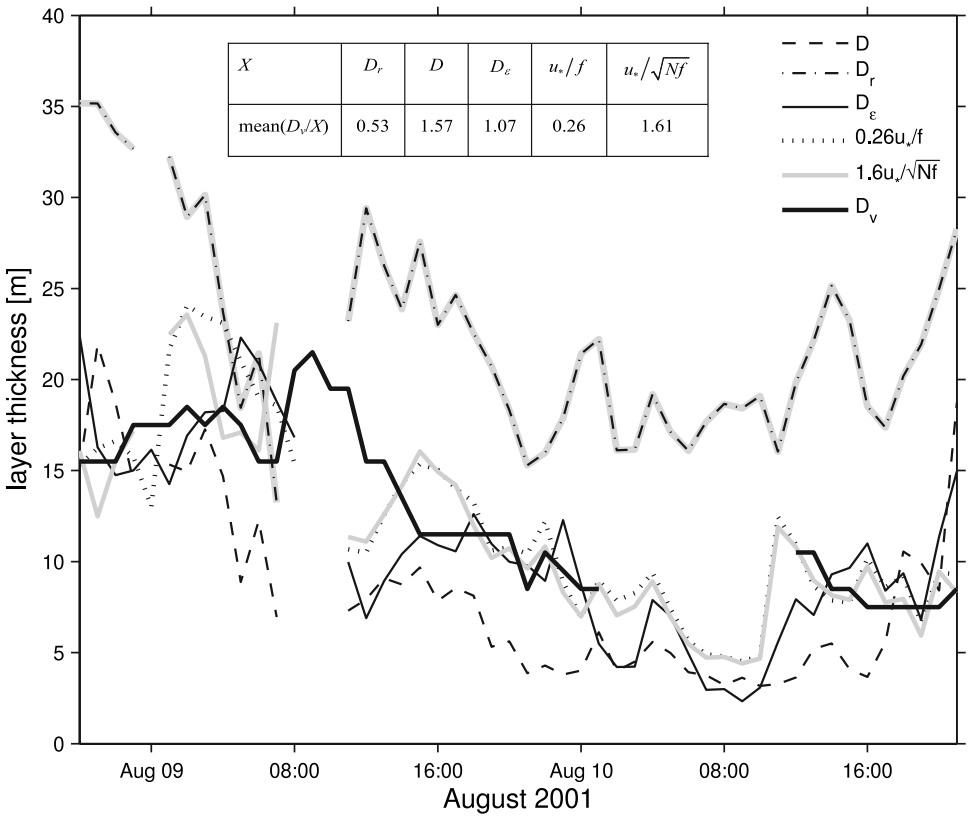

Figure 7. Data from the 50-h Chameleon time series showing the heights of the mixed (D), remnant (D_r), turbulent (D_ε) layers, neutrally stratified Ekman layer scaling $0.26u_*/f$, and positively stratified Ekman layer scaling $1.6u_*/\sqrt{Nf}$. Also shown is the height of the veering layer (D_v) derived from 21 h filtered mooring velocity. D_v is not shown from 10 August 01:00 to 12:00 because current speed was below the threshold chosen for the estimation of the veering layer.

(U_{20} < 15 cm/s, Figure 9c) are statistically insignificant at the 95% confidence limit.

5. Comparison of Observations and Theory

[24] To illustrate the comparison between the observations and the model, a single observed velocity profile is plotted with the theoretical profiles using the viscosity parameterization of the law-of-the-wall (CRM) and the modified law-of-the-wall (MLW) (Figure 10). Both models do not include any fitting parameters. It has been assumed that the entire Ekman transport is contained below $z = D_v$. The values of u_* and h_d used in the model have been computed from the turbulence measurements [see *Perlin et al.*, 2005b]. The value of h_d in this example is almost equal to D_v; turbulent viscosity in the MLW model drops to zero at $z = h_d$ and velocity profiles are not defined above that height. Velocity atop the veering layer is used in place of $\bar{v}$ in the model.

[25] The effect of the stratification in suppressing turbulence at the top of the BBL is clear in the MLW solution where the u-momentum is constrained below h_d. The CRM solution is characterized by weaker u_e and smaller veering angles, but the u-velocity penetrates far above the seafloor. One outcome of the modified law-of-the-wall [*Perlin et al.*, 2005b] has been the good agreement between the modeled and the measured profiles of $\varepsilon(z)$ in the lower 60–70% of the mixed layer. This represents an improvement over the traditional law-of-the-wall which was only good in the lower 20–30% [*Perlin et al.*, 2005b]. In agreement with that result, the velocity and the veering profiles compare with the data relatively well below $0.7D$, but disagree in the upper portion of the mixed layer. The MLW model is not viewed as a complete physical model, but rather as a test of the included physics (particularly, the effect of the stratification cap on the Ekman solution). Its applicability is limited by unresolved processes near the top of the mixed layer (like internal waves and advection). Controlled experiment is required to test the turbulent viscosity profile in the upper part of the bottom boundary layer, and our field data do not satisfy the necessary requirements for the controlled experiment. We have plotted an additional solution (marked MLW2), in which K_v does not drop to zero at h_d, but remains at a small value $K_v = 10^{-3}$ m^2 s^{-1} through the rest of the water column. This value is based on our estimation (from turbulence measurements) of mean K_v in the interior. Non-zero value of K_v above h_d allows the veering to penetrate higher in the water column, which results in a thicker veering layer. This solution does not give much improvement over the original MLW and the tested parameterization of K_v in the interior does not reflect any real

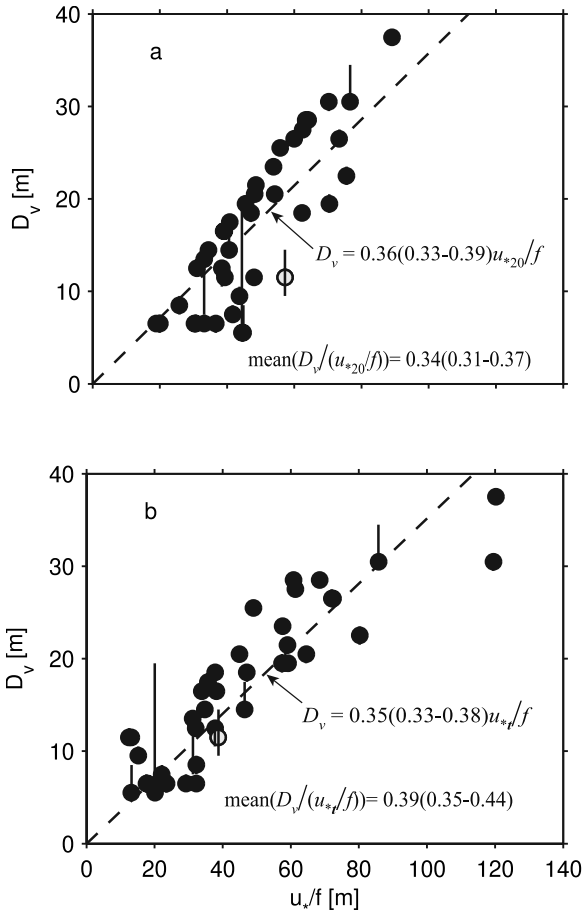

Figure 8. Veering layer height from moored velocity is plotted as a function of friction velocity (a) u_{*20} and (b) u_{*t}. Uncertainties for the veering layer height are based on 4° and 8° thresholds. Linear regression is shown by dashed line. 95% confidence limits are shown in brackets. Gray dots are the data from the 50-h time series (Figure 7).

physics. For further analysis we opted for a zero K_v above h_d.

[26] Note that all model solutions (CRM, MLW and MLW2) have the same transport perpendicular to $\bar{v}$ as required by the integral of (2), which in this example is not identical to the measured transport. Mean values of the friction velocities computed from the transport and from the turbulence data agree statistically and are highly correlated [*Perlin et al.*, 2005a, Figure 14], while they could differ for a particular profile.

[27] We have then compared the entire 50-h Chameleon time series observations with the MLW model (Figure 11). We have not plotted the model solution above 0.7D, since we do not expect to see the agreement with the data in that region. During the 50-h time series the turbulence measurements have been used to estimate u_* and h_d directly. As previously discussed, for the purpose of data analysis we have assumed that the entire transport perpendicular to $\bar{v} = v(D_v)$ occurs below $z = D_v$. MLW provides a relatively good fit in the lower half of the boundary layer and predicts magnitudes of u_e and veering angles.

[28] Comparison of the moored observations and the MLW model for the entire 3-month time series has shown similar results (Figure 12). Here u_{*20} has been estimated from a drag coefficient $C_D = 10^{-3}$ and observed U_{20} [see *Perlin et al.*, 2005b, Figure 4]. To apply the MLW model, we have assumed that $h_d = D_v$. Again, the MLW model

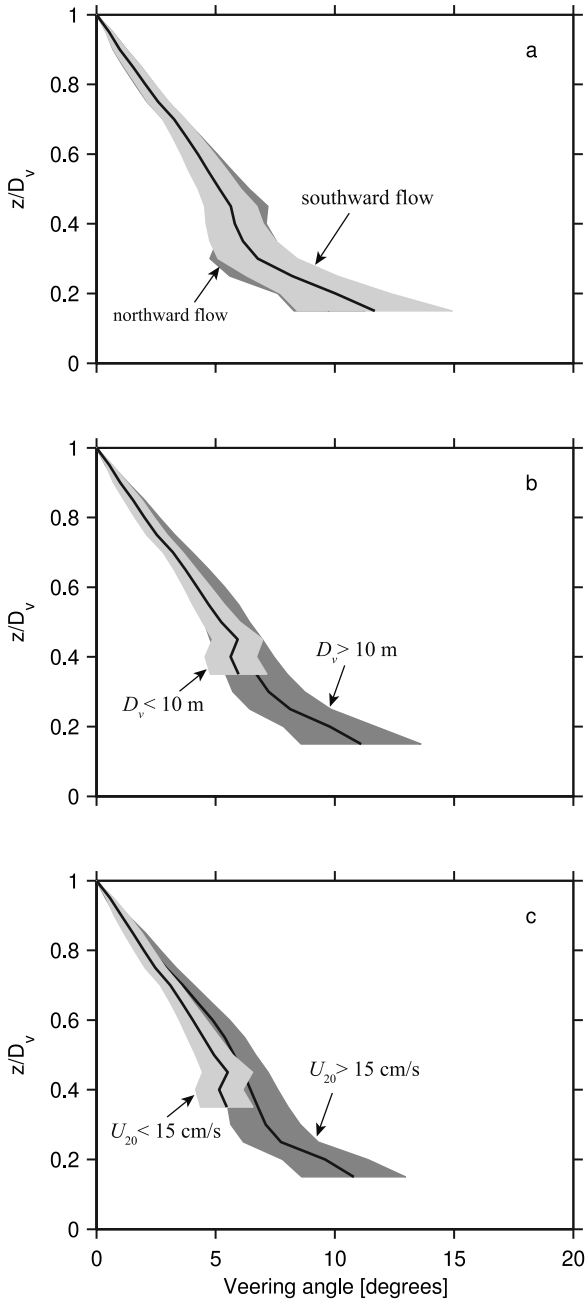

Figure 9. Average veering angle profiles $\alpha_{av}(z/D_v)$ (with 95% confidence limits) versus nondimensionalized height above the bottom. (a) Veering angle for northward (dark gray) and southward (light gray) flow; (b) veering angle for thick (>10 m, dark gray) and thin (<10 m, light gray) veering layers; (c) veering angle for fast current (U_{20} > 15 cm s^{-1}, dark gray) and slow current (U_{20} <15 cm s^{-1}, light gray). The veering angles for thin veering layers and for slow velocities on (b) and (c) are truncated due to shadow zone of ADCP combined with normalization of z by D_v.

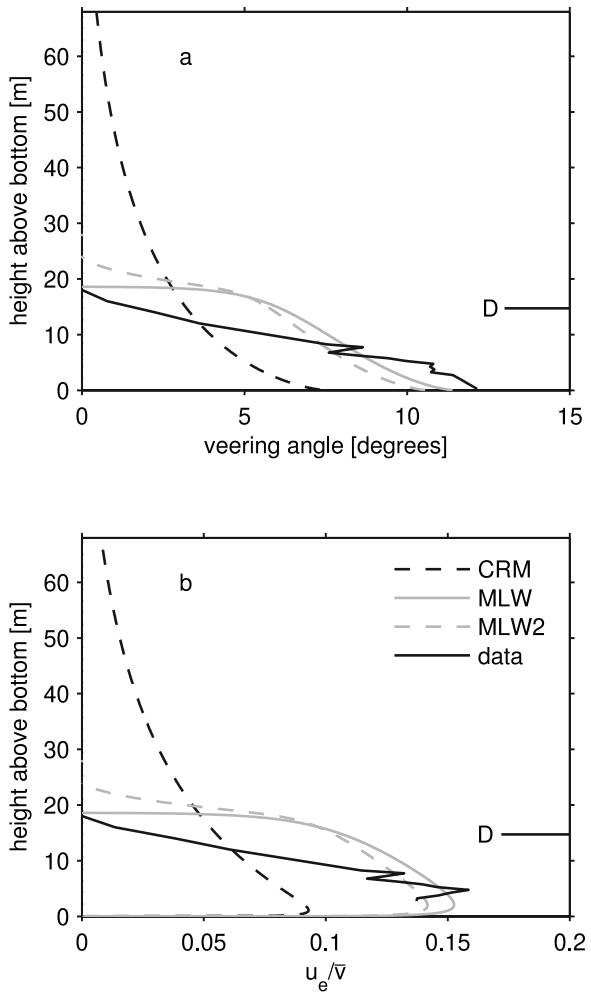

Figure 10. Comparison of CRM and MLW models with sample Chameleon profile in Figure 3 showing (a) veering angle and (b) u_e component of velocity. In this example velocity at D_v, $\overline{v} = 0.21$ m s^{-1}, $u_* = 7{\cdot}10^{-3}$ m s^{-1}, and $h_d =$ 18.6 m. The MLW model has a cap on the lengths scale of turbulence set by the level of turbulence and the stratification above the mixed layer (see text). MLW2 is a modification of MLW, in which turbulent viscosity does not drop below 10^{-3} m^2 s^{-1} above the mixed layer.

shows reasonable agreement with the data, slightly underpredicting the veering angle in the lower part of the profile.

[29] While the gross characteristics of the observations are captured by MLW, some of the comparisons are obscured by the averaging in Figures 11 and 12. The maximum veering angle in the MLW model depends on $\overline{v}$, so that the greater the interior current the stronger the veering. The data are too limited to demonstrate this relationship in any meaningful way.

6. Summary

[30] Observations reveal a systematic counter-clockwise rotation with depth of the daily averaged current over three summer months on the Oregon shelf, except during periods of low speed or immediately following a reversal of alongshore velocity (Figure 9). The velocity profile near the bottom shows the maximum veering of 12° (Figure 9). This is much less than the 45° of the classic Ekman solution (constant K_v), but is in the range of the other BBL measurements (Table 1). The maximum veering angle has only a very weak dependence on the interior flow velocity and the thickness of the veering layer. The thickness of the veering layer D_v does not appear to depend on the flow direction, regardless of whether the Ekman transport is upslope for southward interior flow, or downslope for northward interior flow (Figure 9).

[31] For a 50-h segment during which our measurements of the velocity were supplemented by intensive turbulence and density profiles, we have found that the veering layer height is nearly equal to the turbulent boundary layer height. This is consistent with the result described by *Perlin et al.* [2005a], who have shown that the cross-shore movement of the fluid in the BBL is well-modeled by the measured friction velocity (u_*) and the momentum distributed over

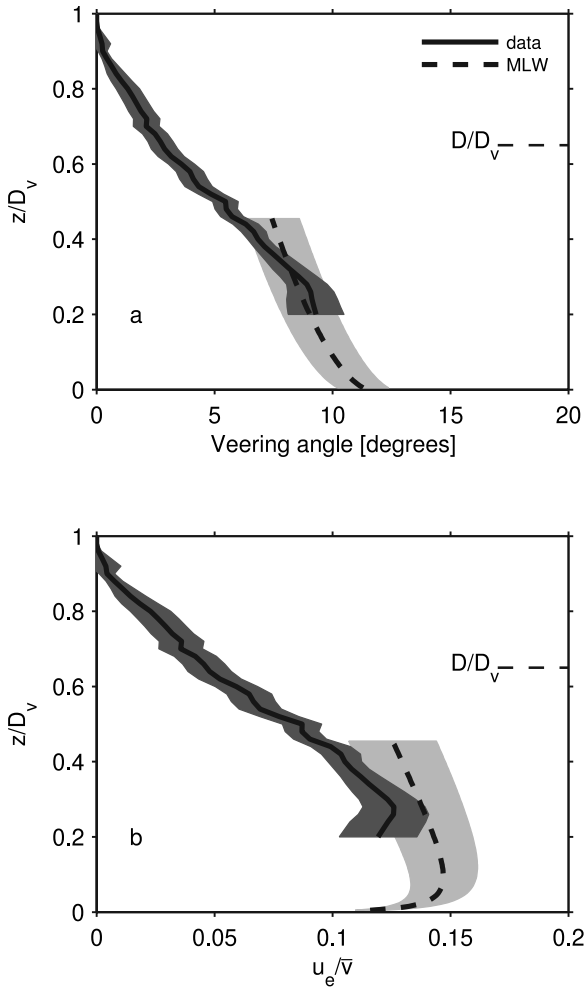

Figure 11. Comparison of (a) veering angle and (b) u_e for MLW model and observations from 50-h Chameleon time series. Profiles are nondimensionalized by the thickness of the veering layer, D_v. Model is computed with measured $\overline{v}$ and u_* estimated from turbulence data. The parameter h_d for the MLW model is computed from the turbulence and density distribution. Shaded area represents 95% confidence limits. D/D_v marks the mean ratio of mixed and veering layer heights for the 50-h time series.

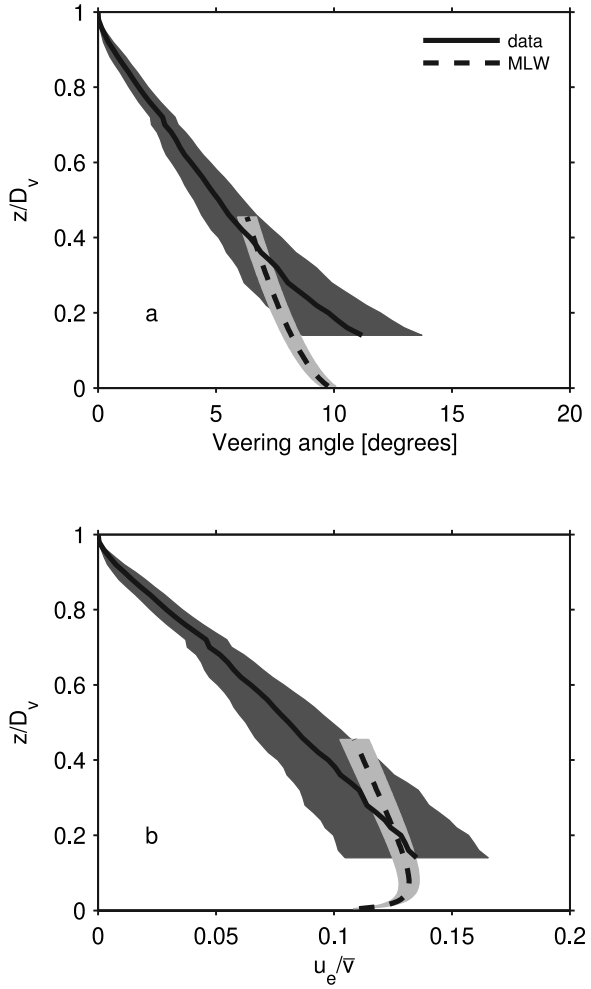

Figure 12. Comparison of (a) veering angle and (b) u_e for MLW model and observations from the three-month moored time series. Profiles are nondimensionalized by the thickness of the veering layer, D_v. Model is computed with measured $\bar{v}$ and u_{*20}; the parameter h_d is taken to be equal to D_v. Shaded area represents 95% confidence limits.

a turbulent layer height, D_ε. This and the high near-bottom velocities presented here clearly demonstrate that the Ekman spiral is confined to the turbulent layer near the seafloor in a stratified ocean. We also expect that the thickness of the bottom turbulent layer depends on the time history of the turbulence, the background stratification, and the speed with which fluid mixed in the BBL is flushed either by geostrophic adjustment or by ambient currents. For instance, *Moum et al.* [2004] have found that the turbulence in the boundary layer transitions from being driven by stress during upwelling, to being driven by convection during downwelling. It seems unlikely that the thickness of the veering layer would scale in the same way for both regimes.

[32] The veering layer apparently is further constrained to within the weakly stratified remnant layer ($D_r \cong 2D_v$) although it is thicker than the mixed layer immediately adjacent to the sea floor ($D \cong 2/3D_v$). 90% of the Ekman transport have been found within this bottom mixed layer. While this result may seem to contradict the corresponding results for the surface Ekman layer [*Weller and Plueddemann*, 1996], the structural differences in the spirals, one a surface-forced veering with depth-decaying cross-axis velocity magnitude and the other with a near-bottom cross-axis velocity maximum, make these difficult to compare without a model that properly accounts for the turbulence (eddy viscosity) and stratification throughout the full extent of the Ekman layer.

[33] The velocity profile near the bottom is approximated by the Ekman balance between Coriolis and friction stresses in the boundary layer using the turbulent viscosity K_v derived from the MLW, which takes into account the suppression of turbulent motion by stratification at the top of the mixed layer [*Perlin et al.*, 2005b] (Figures 11 and 12). The MLW model approximates velocity and veering relatively well in the lower half of the veering layer. The model, however, does not fit well near the top of the mixed layer, where it requires the turbulent viscosity drop to zero. If the classic law-of-the-wall (CRM) is used for the turbulent viscosity, we find that the Ekman transport is distributed over a much thicker layer than in the observations, and the veering of the velocity near the bottom is underpredicted (Figure 10).

[34] The Ekman lengths scales u_*/f and $u_*/\sqrt{Nf}$ appear to relate to D_v within accepted constants (Figure 7 and *Pollard et al.* [1973], respectively). Our measurements do not permit an evaluation of the influence of the latitude changes on the Ekman layer height. The model suggests dependence of layer height on rotation. However, the presence of stratification, presumably imposed by unrelated mesoscale processes, may lock the bottom Ekman layer in a thin boundary layer even at low latitudes. The analysis of the effect of rotation in the presence of stratification seems an important problem to address.

[35] **Acknowledgments.** We are grateful to Mike Neeley-Brown, Ray Kreth, Grieg Thompson, and Gunnar Gunderson for their engineering contributions to Chameleon and for their help in collecting the data. The captain and crew of the R/V *T. G. Thompson* were helpful in all regards. Thanks also to Walt Waldorf and Steve Gard for their roles in deploying the moorings and processing the data. This work was funded by the National Science Foundation (grant 9907854).

References

Barth, J. A., and P. A. Wheeler (2005), Introduction to special section: Coastal Advances in Shelf Transport, *J. Geophys. Res.*, *110*, C10S01, doi:10.1029/2005JC003124.

Boyd, T., M. D. Levine, P. M. Kosro, S. R. Gard, and W. Waldorf (2002), Observations from moorings on the Oregon continental shelf, May–August 2001, *Data Rep. 190 2002–6*, Oregon State Univ., Corvallis.

Cushman-Roisin, B. (1994), *Introduction to Geophysical Fluid Dynamics*, 320 pp., Prentice-Hall, Upper Saddle River, N. J.

Cushman-Roisin, B., and V. Malačič (1997), Bottom Ekman pumping with stress-dependent eddy viscosity, *J. Phys. Oceanogr.*, *27*, 1967–1975.

Dewey, R. K., and W. R. Crawford (1988), Bottom stress estimates from vertical dissipation rate profiles on the continental shelf, *J. Phys. Oceanogr.*, *18*, 1167–1177.

Dickey, T. D., and J. C. Van Leer (1984), Observations and simulation of a bottom Ekman layer on a continental shelf, *J. Geophys.*, *89*, 1983–1988.

Ellison, T. H. (1956), Atmospheric turbulence, in *Surveys in Mechanics, G.I. Taylor Anniversary Volume*, edited by G. K. Batchelor and R. M. Davies, pp. 400–430, Cambridge Univ. Press, New York.

Garrett, C., P. MacCready, and P. Rhines (1993), Boundary mixing and arrested Ekman layers: Rotating stratified flow near a sloping boundary, *Annu. Rev. Fluid Mech.*, *25*, 291–323.

Huyer, A., and R. L. Smith (1978), Seasonal differences in low-frequency current fluctuations over the Oregon continental shelf, *J. Geophys. Res.*, *83*, 5077–5089.

Kundu, P. K. (1976), Ekman veering observed near the ocean bottom, *J. Phys. Oceanogr.*, *6*, 238–242.

Lass, H. U., and V. Mohrholz (2003), On dynamics and mixing of inflowing saltwater in the Arkona Sea, *J. Geophys. Res.*, *108*(C2), 3042, doi:10.1029/2002JC001465.

Madsen, O. S. (1977), A realistic model in the wind-induced Ekman boundary layer, *Phys. Oceanogr.*, *7*, 248–255.

Mercado, A., and J. Van Leer (1976), Near bottom velocity and temperature profiles observed by cyclesonde, *Geophys. Res. Lett.*, *3*, 633–636.

Moum, J. N., M. C. Gregg, R. C. Lien, and M. E. Carr (1995), Comparison of turbulence kinetic energy dissipation rate estimates from two ocean microstructure profilers, *J. Atmos. Oceanic Technol.*, *12*, 346–366.

Moum, J. N., A. Perlin, J. M. Klymak, M. D. Levine, T. Boyd, and P. M. Kosro (2004), Convectively-driven mixing in the bottom boundary layer over the continental shelf during downwelling, *J. Phys. Oceanogr.*, *34*, 2189–2202.

Perlin, A., J. N. Moum, and J. M. Klymak (2005a), Response of the bottom boundary layer over a sloping shelf to variations in alongshore wind, *J. Geophys. Res.*, *110*, C10S09, doi:10.1029/2004JC002500.

Perlin, A., J. N. Moum, J. M. Klymak, M. D. Levine, T. Boyd, and M. Kosro (2005b), A modified law-of-the-wall to describe velocity profiles in the oceanic bottom boundary layers, *J. Geophys. Res.*, *110*, C10S10, doi:10.1029/2004JC002310.

Pollard, R. T., P. B. Rhines, and R. O. R. Y. Thompson (1973), The deepening of the wind-mixed layer, *Geophys. Fluid Dyn.*, *3*, 381–404.

Price, J. F., and M. A. Sundermeyer (1999), Stratified Ekman layers, *J. Geophys. Res.*, *104*(C9), 20,467–20,494.

Saylor, J. H. (1994), Studies of bottom Ekman layer processes and mid-lake upwelling in the Laurentian Great Lakes, *Water Pollut. Res. J. Can.*, *29*, 233–246.

Saylor, J. H., and G. M. Miller (1988), Observation of Ekman veering at the bottom of Lake Michigan, *J. Great Lakes Res.*, *14*, 94–100.

Weatherly, G. L. (1972), A study of the bottom boundary layer of the Florida current, *J. Phys. Oceanogr.*, *2*, 54–72.

Weller, R. A., and A. J. Plueddemann (1996), Observations of the vertical structure of the oceanic boundary layer, *J. Geophys. Res.*, *101*, 8789–8806.

T. Boyd, P. M. Kosro, M. D. Levine, J. N. Moum, and A. Perlin, College of Oceanic and Atmospheric Sciences, Oregon State University, Corvallis, OR 97331-5503, USA. (aperlin@coas.oregonstate.edu)

J. M. Klymak, School of Earth and Ocean Sciences, Department of Physics, University of Victoria, Victoria, BC, Canada V8W 3P6.